European Journal of Mechanics / A Solids 115 (2026) 105832

Contents lists available at ScienceDirect

European Journal of Mechanics / A Solids

journal homepage: www.elsevier.com/locate/ejmsol

Full length article

A novel analytical beam formulation and its application on composite wind turbine blades

Mertol Tüfekci [a,b,*], Ekrem Tüfekci [c]

[a] Centre for Engineering Research, University of Hertfordshire, Hatfield AL10 9AB, UK
[b] School of Physics, Engineering and Computer Science, University of Hertfordshire, Hatfield AL10 9AB, UK
[c] Faculty of Mechanical Engineering, İstanbul Technical University, İstanbul, 34437, Turkiye

ARTICLE INFO

Keywords:
Non-uniform and asymmetrical beams
Functionally graded materials and composites
Analytical solution
Composite wind turbine blades
Static behaviour

ABSTRACT

This paper presents a novel analytical formulation for modelling the mechanics of non-uniform and asymmetrical straight beams made of functionally graded materials (FGMs) and composites. This approach addresses the complexities caused by the asymmetry of the cross-section and those arising from the variations in geometry and material properties along the beam's axis by approximating these variations as stepped changes. It is assumed that each segment of the beam has constant properties, which are determined through the averaging of functions representing the actual property variations. This method enables efficient and accurate modelling/representation of beam structures such as wind turbine blades. The accuracy and reliability of the analytical model are verified through a comparison with the Technical University of Denmark (DTU) 10 MW reference wind turbine blade, considering two representative load cases (bending, BLC1 and torsional, BLC2) and confirming its ability to accurately predict the structural response. Furthermore, the study assesses the computational performance of the model, demonstrating its efficiency. This study contributes to the literature by providing a robust and computationally efficient approach for the analysis of wind turbine blades.

1. Introduction

Wind turbine blades are essential components in wind energy systems, significantly influencing the efficiency and performance of turbines. The design and analysis of these blades are challenging due to the necessity for high-strength, lightweight structures capable of withstanding various dynamic and static loads as well as ensuring good aerodynamic performance (Liu et al., 2022b,a; Liu, 2021; Tüfekci, 2023). The aerodynamic performance requirement significantly constrains the design of the outer geometry of the blade and leaves the internal support and material selection as design variables for the solid mechanics part of the design problem (Van Buren and Atamturktur, 2012; Buckney et al., 2013; Zheng et al., 2023; Tüfekci et al., 2025; Jiang et al., 2022a). Hence, composite materials, known for their superior mechanical properties, are commonly used in manufacturing these blades. Due to the loading and operating conditions on the blades, different mechanical requirements are present for different parts of the blade, necessitating the use of various composite materials tailored to these specific demands. Making such design decisions requires a deep understanding of the blade's mechanical behaviour, but creating full-scale models can be time-consuming, effort-intensive, and computationally expensive. Therefore, modelling blades as beams and shells is a sensible and beneficial approach, balancing between computational efficiency and the ability to capture the essential mechanical responses of the structure. However, to represent such complicated geometries with beams is challenging due to a set of factors including the geometry of the cross-section and material properties (Couturier and Krenk, 2016; Tüfekci et al., 2020). Therefore,advanced beam theories are usually needed (Tüfekci et al., 2020; Branner et al., 2012; Blasques et al., 2016; Blasques, 2012).

The implementation of advanced beam models is a sound strategy for structural analysis, combining two-dimensional cross-sectional analyses with one-dimensional beam analysis. This method has the potential to significantly reduce computational costs (Natarajan et al., 2012; Branner et al., 2012; Artan and Tepe, 2025a,b; Tepe, 2025). Additionally, tools like BEam Cross-section Analysis Software (BECAS) and Variational Asymptotic Beam Sectional Analysis (VABS) offer robust frameworks for the analysis of anisotropic and inhomogeneous beam sections. These tools, which have been rigorously validated against both experimental and numerical methods, are necessary for accurately modelling the complex structures of wind turbine blades, thereby enhancing the precision and reliability of structural analyses (Blasques, 2012; Yu et al., 2012; Yu, 2011). Finite element (FE) modelling has

* Corresponding author at: Centre for Engineering Research, University of Hertfordshire, Hatfield AL10 9AB, UK.
E-mail address: m.tufekci@herts.ac.uk (M. Tüfekci).

https://doi.org/10.1016/j.euromechsol.2025.105832
Received 3 October 2024; Received in revised form 27 July 2025; Accepted 9 August 2025
Available online 19 August 2025

been demonstrated to be an effective approach for analysing the structural characteristics of composite wind turbine blades, enabling a comprehensive examination of stress, strain, and deformation under static and dynamic loads (Bechly and Clausen, 1997; Liu et al., 2022b,a; Zheng et al., 2023; Eder and Bitsche, 2015).

Non-linear beam theory, extended from Euler–Bernoulli to Timoshenko beam theory, demonstrates high computational accuracy and efficiency, effectively modelling bend-twist coupling due to material anisotropy and geometry as well as considering large deformation non-linearity (Zhou et al., 2018; Genel and Tüfekci, 2023b,a; Mohamad Mirfatah et al., 2024; Tüfekci, 2025; Tüfekci et al., 2024b,a). Three-dimensional analytical beam models for the dynamic analysis of blades made of fibre-reinforced composites show close agreement between analytical and FE modelling results, achieving an accurate modelling of the blade dynamics while remaining computationally very efficient (Tüfekci et al., 2020).

Dynamic and aeroelastic analyses using thin-walled composite beam and continuum models reveal important coupling effects and validate natural frequencies and mode shapes under various operational conditions (Yilmaz et al., 2014; Chang et al., 2020; Guo et al., 2020; Peng et al., 2024; Jiang et al., 2022b). Comprehensive FE modelling methods simulate multiple failure modes in composite box beams, which are also thin-walled structures that are beneficial in understanding the failure behaviour of wind turbine blades under various loading conditions as some wind turbine blade designs consist of beams with box profiles (Chen et al., 2019; Ozyildiz et al., 2018). Geometric non-linear analyses of composite beams using advanced parameterisation methods help in understanding the effects of large deformations and rotation in structural analysis. These are usually seen in such wind turbine blade systems and should be considered for realistic models (Wang and Yu, 2017).

Sandwich materials are utilised in wind turbine blades due to their high specific stiffnesses and specific strengths, significantly improving performance and durability under various load conditions (Thomsen, 2009; Tüfekci et al., 2023). The optimisation of resin uptake in the skin/core interphase region of 3D-printed core sandwich composites further illustrates the potential for enhanced bending and shear performance in such materials (Cao et al., 2023). Composite materials, including glass and carbon fibres, are extensively used for their superior mechanical properties and lightweight characteristics (Schubel and Crossley, 2012; Brøndsted et al., 2005; Spini and Bettini, 2024). Optimising the structural design of wind turbine blades requires the use of various computational and analytical methods to enhance performance and reduce material costs. FE analysis plays a pivotal role in this process, providing detailed and accurate results regarding the stress and strain distribution within the blade structure (Theotokoglou and Balokas, 2014; Kong et al., 2005).

Comparative studies of different modelling approaches, including geometrically-exact beam and shell elements, highlight the strengths and limitations of each method. These comparisons are essential for selecting the most appropriate modelling technique for specific design and analysis requirements (Júnior et al., 2019; Cardenas et al., 2011; Tüfekci et al., 2020). For instance, modelling wind turbine blades using geometrically-exact beam and shell elements shows that these models present very similar global behaviour, though shell models reveal local buckling phenomena that may significantly impact the novel blade designs (Faccio Júnior et al., 2019).

In the broader context of composite materials and their applications in similar structural components, several studies can be found in the literature. Research on fibre ply design for aero engine composite fan blades demonstrates the impact of different ply orientation patterns on the reliability and vibration characteristics of the blades (Xiao et al., 2017). Additionally, structural optimisation of composite wind turbine blades using genetic algorithms and FE analysis shows significant potential for weight reduction and performance enhancement (Barnes and Morozov, 2016; Fagan et al., 2017; Wang et al., 2016).

The mechanical performance of balsa wood and its sandwich structures is another area of interest, particularly for applications requiring high specific stiffnesses and specific strengths (Tüfekci et al., 2023). The use of analytical and numerical simulation and FE analysis to identify areas of weakness and optimise composite wind turbine blades underscores the importance of advanced modelling techniques (Raman et al., 2016; Tarfaoui et al., 2020; Liu et al., 2022b; Uzun et al., 2024). Multiobjective optimisation of composite wind turbine blades highlights the need to balance material properties and geometric design to achieve cost-effective and high-performance structures (Jureczko and Mrówka, 2022). The development of damped structural dynamics models for large wind turbine blades, including material and structural damping, contributes to expand the understanding of the dynamic behaviour of these structures (Chortis et al., 2007).

Static and free vibration analyses of functionally graded material beams using modified Timoshenko beam theory and other advanced methods, including higher order beam theories that can provide a comprehensive understanding of the mechanical behaviour of these materials under various loading conditions (Katili et al., 2020; Filippi et al., 2015; Guan et al., 2023; Li et al., 2014; Hadji et al., 2021; Avcar et al., 2021).

In this context, this research contributes to the field of mechanics by presenting a novel analytical framework designed to model the mechanics of beams with asymmetric cross-sections and varying geometry and material properties along their axis. The approach addresses the complexity of variation by employing a stepped approximation, where each segment of the beam is assumed to have constant properties derived from averaging functions that represent actual variations (Tüfekci et al., 2020; Tufekci and Ozdemirci, 2006; Tufekci and Dogruer, 2002, 2006). This stepped approximation allows for the discretisation of the beam into manageable segments, simplifying the analysis and making it possible to achieve an analytical solution while maintaining a high level of accuracy. By capturing the variations in geometry and material properties, the framework effectively models the complex interactions within the beam structure under static loading conditions, including cases involving concentrated loads. This capability is particularly important for components like wind turbine blades, which are subjected to diverse and significant forces. Additionally, the model lends itself well to comparison with high-fidelity numerical analyses, supporting its accuracy and applicability. The proposed model's performance is validated using the Technical University of Denmark (DTU) 10 MW reference wind turbine blade, demonstrating its accuracy and applicability to wind turbine blades and other complex structures. The validation process includes comprehensive comparisons with established numerical methods, showing that the analytical model can achieve similar levels of accuracy while significantly reducing computational time, resource requirements, and pre-processing effort. Owing to its non-complex theoretical foundation, the method provides practical advantages in terms of implementation and performance, making it a suitable alternative for the structural analysis of complex beam-like components. The model provides significant advantages, including the ability to handle complex geometries and material distributions with reduced computational costs compared to more detailed FE methods. The smooth transitions between segments, ensured by the model's formulation, enhance the overall fidelity of the simulation, making it a practical and robust tool for engineers working on advanced structural designs. Ultimately, this research contributes to the broader field of structural analysis by introducing a method that provides theoretical simplicity and computational efficiency, enabling accurate and practical modelling of composite beams and blades, as well as other complex systems that can be represented using beam formulations.

2. Analytical formulation of the beam

This section presents the analytical formulation required to describe the mechanical behaviour of a beam with non-uniform and asymmetric

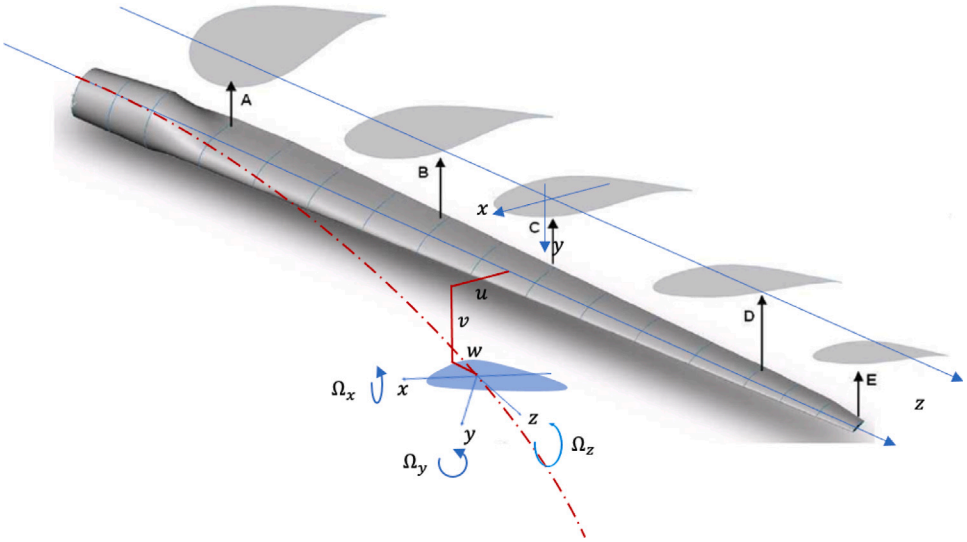

Fig. 1. Schematic representation of the blade geometry, coordinate system, displacement components (u, edgewise, v, flapwise, w, axial), and rotation components (Ω_x, Ω_y, Ω_z).

characteristics. The formulation incorporates the fundamental principles of equilibrium, compatibility, and constitutive relations in order to establish a comprehensive framework for analysing beams with varying material properties and geometric configurations along their length. By deriving the equilibrium equations, compatibility conditions, and constitutive relationships in a systematic manner, a set of combined equations governing the beam's response under various loading conditions is constructed. These equations are then represented in matrix form in order to permit further analysis and numerical implementation.

Fig. 1 illustrates the coordinate system and loading directions used in this study. The local (x, y, z) coordinate system is defined such that the z-axis lies along the blade (beam) span. The displacement components u, v, w correspond to edgewwise, flapwise, and axial directions, respectively. Similarly, Ω_x, Ω_y, Ω_z represent the rotations about the respective axes. The figure also shows the typical application points and directions of loads, which are referenced in the following derivation of the equilibrium equations.

The analytical formulation developed in this study is grounded in the Timoshenko beam theory, which provides an accurate representation, particularly for beams with moderate slenderness. The model assumes small deformations and linear elastic material behaviour throughout the structure. Classical assumptions associated with Timoshenko theory are adopted, including the preservation of cross-sectional rigidity, meaning each cross section remains planar and undistorted during deformation, and allowance for shear deformation by introducing transverse shear strains. These assumptions enable the inclusion of both bending and shear effects in the analysis, which are essential for accurately modelling complex structures like wind turbine blades that may exhibit significant transverse shear. The theory therefore provides a robust and computationally efficient framework for capturing the coupled axial, bending, shear, and torsional responses of composite and functionally graded blades.

2.1. Equilibrium equations

The equilibrium equations are given below:

$$\frac{dF_x}{dz} + q_x = 0 \tag{1}$$

$$\frac{dF_y}{dz} + q_y = 0 \tag{2}$$

$$\frac{dF_z}{dz} + q_z = 0 \tag{3}$$

$$\frac{dM_x}{dz} - F_y + m_x = 0 \tag{4}$$

$$\frac{dM_y}{dz} + F_x + m_y = 0 \tag{5}$$

$$\frac{dM_z}{dz} + m_z = 0 \tag{6}$$

where q_x, q_y, and q_z are the distributed external forces; m_x, m_y, and m_z are the distributed external moments; F_x, F_y, and F_z are the internal force resultants; and M_x, M_y, and M_z are the internal moment resultants.

2.2. Compatibility equations

The compatibility conditions of the beam are described by the following equations:

$$\frac{du}{dz} - \Omega_y - \varepsilon_{xz} = 0 \tag{7}$$

$$\frac{dv}{dz} + \Omega_x - \varepsilon_{yz} = 0 \tag{8}$$

$$\frac{dw}{dz} - \varepsilon_{zz} = 0 \tag{9}$$

$$\frac{d\Omega_x}{dz} - \omega_x = 0 \tag{10}$$

$$\frac{d\Omega_y}{dz} - \omega_y = 0 \tag{11}$$

$$\frac{d\Omega_z}{dz} - \omega_z = 0 \tag{12}$$

where ω_x, ω_y, and ω_z represent the curvature components of the deformed beam axis, ε_{xz} and ε_{yz} denote transverse shear strains and ε_{zz} represents the axial strain.

2.3. Constitutive equations

Under the assumptions of linear elastic material properties, the constitutive equations are given by:

$$\begin{bmatrix} F_x \\ F_y \\ F_z \end{bmatrix} = \begin{bmatrix} GAk_x & 0 & 0 \\ 0 & GAk_y & 0 \\ 0 & 0 & EA \end{bmatrix} \begin{bmatrix} \varepsilon_{xz} \\ \varepsilon_{yz} \\ \varepsilon_{zz} \end{bmatrix} \tag{13}$$

$$\begin{bmatrix} M_x \\ M_y \\ M_z \end{bmatrix} = \begin{bmatrix} EI_x & -EI_{xy} & 0 \\ -EI_{xy} & EI_y & 0 \\ 0 & 0 & GI_t \end{bmatrix} \begin{bmatrix} \omega_x \\ \omega_y \\ \omega_z \end{bmatrix} \tag{14}$$

where A is the cross-sectional area; I_x and I_y are the moments of inertia; I_{xy} is the product moment of inertia; I_t is the torsional constant; k_x and k_y are shear correction factors; and E and G are the Young's and shear moduli, respectively.

$$\mathbf{A} = \begin{bmatrix} 0 & 0 & 0 & 0 & 1 & 0 & \frac{1}{GAk_x} & 0 & 0 & 0 & 0 & 0 \\ 0 & 0 & 0 & -1 & 0 & 0 & 0 & \frac{1}{GAk_y} & 0 & 0 & 0 & 0 \\ 0 & 0 & 0 & 0 & 0 & 0 & 0 & 0 & \frac{1}{EA} & 0 & 0 & 0 \\ 0 & 0 & 0 & 0 & 0 & 0 & 0 & 0 & 0 & \frac{I_y}{E(I_xI_y-I_{xy}^2)} & \frac{I_{xy}}{E(I_xI_y-I_{xy}^2)} & 0 \\ 0 & 0 & 0 & 0 & 0 & 0 & 0 & 0 & 0 & \frac{I_{xy}}{E(I_xI_y-I_{xy}^2)} & \frac{I_x}{E(I_xI_y-I_{xy}^2)} & 0 \\ 0 & 0 & 0 & 0 & 0 & 0 & 0 & 0 & 0 & 0 & 0 & \frac{1}{GI_t} \\ 0 & 0 & 0 & 0 & 0 & 0 & 0 & 0 & 0 & 0 & 0 & 0 \\ 0 & 0 & 0 & 0 & 0 & 0 & 0 & 0 & 0 & 0 & 0 & 0 \\ 0 & 0 & 0 & 0 & 0 & 0 & 0 & 0 & 0 & 0 & 0 & 0 \\ 0 & 0 & 0 & 0 & 0 & 0 & 0 & -1 & 0 & 0 & 0 & 0 \\ 0 & 0 & 0 & 0 & 0 & 0 & 1 & 0 & 0 & 0 & 0 & 0 \\ 0 & 0 & 0 & 0 & 0 & 0 & 0 & 0 & 0 & 0 & 0 & 0 \end{bmatrix} \tag{23}$$

Box I.

It is important to note that both Eqs. (13) and (14) are expressed as functions of the beam axis coordinate z, meaning that the internal force and moment resultants on the left-hand sides, as well as the corresponding strain and curvature quantities on the right-hand sides, represent their respective values at a given z coordinate along the beam. This spatial dependence allows the formulation to account for the non-uniform characteristics of the structure.

2.4. Combined equations

The combined equations derived from the equilibrium and compatibility equations, along with the constitutive relationships, are well known as:

$$\frac{du}{dz} = \Omega_y + \frac{F_x}{GAk_x} \tag{15}$$

$$\frac{dv}{dz} = -\Omega_x + \frac{F_y}{GAk_y} \tag{16}$$

$$\frac{dw}{dz} = \frac{F_z}{EA} \tag{17}$$

$$\frac{d\Omega_x}{dz} = \frac{M_x}{E}\left(\frac{I_y}{I_xI_y - I_{xy}^2}\right) + \frac{M_y}{E}\left(\frac{I_{xy}}{I_xI_y - I_{xy}^2}\right) \tag{18}$$

$$\frac{d\Omega_y}{dz} = \frac{M_x}{E}\left(\frac{I_{xy}}{I_xI_y - I_{xy}^2}\right) + \frac{M_y}{E}\left(\frac{I_x}{I_xI_y - I_{xy}^2}\right) \tag{19}$$

$$\frac{d\Omega_z}{dz} = \frac{M_z}{GI_t} \tag{20}$$

2.5. System representation and solution method for beam analysis

2.5.1. System representation

Eqs. (15)–(20) and (1)–(6) are used to formulate the system of 12 first-order ordinary differential equations with 12 variables, which govern the beam's static response and are expressed compactly in matrix form:

$$\frac{d\mathbf{y}}{dz} = \mathbf{A}\mathbf{y} \tag{21}$$

where $\mathbf{y}$ is the state vector given by:

$$\mathbf{y}^T = \left[u, v, w, \Omega_x, \Omega_y, \Omega_z, F_x, F_y, F_z, M_x, M_y, M_z\right] \tag{22}$$

and $\mathbf{A}$ is the system matrix, which is shown by the equation in Box I.

The solution of the differential equation given in Eq. (21) is expressed as:

$$\mathbf{y}(z) = \mathbf{Y}(z, z_0)\mathbf{y}_0 \tag{24}$$

Here, $\mathbf{Y}(z, z_0)$ denotes the fundamental solution matrix, and $\mathbf{y}_0$ represents the initial value vector. If $\mathbf{A}$ is constant, representing a beam with constant cross-sectional and material properties, Eq. (24) can be explicitly written using the matrix exponential as:

$$\mathbf{y}(z) = e^{\mathbf{A}z}\mathbf{y}_0 \tag{25}$$

In this context, $\mathbf{Y}(z, z_0) = e^{\mathbf{A}z}$ provides the exact solution of Eq. (21) under the assumption of constant coefficients.

Hence, $\mathbf{Y}$ is given by the equation in Box II.

2.5.2. Analytical solution

The system of differential equations represented by Eq. (21) is analytically solvable when cross-sectional and material properties are constant. However, beams often exhibit variable properties along their length. To address these variations, the proposed approach segments the beam into regions with constant properties, enabling accurate approximation of the beam's behaviour.

The segmentation divides the beam into multiple sections, each with averaged geometric and material properties based on the average value theorem. This transforms the complex variable-property problem into manageable sub-problems whilst maintaining an accurate representation of the beam's characteristics.

To apply the segmentation, the domain is divided into n segments, with segment boundaries defined by:

$$\begin{aligned} z_0 &= 0, \quad z_1 = \frac{l}{n}, \quad \ldots, \quad z_{i-1} = \frac{(i-1)l}{n}, \\ z_i &= \frac{il}{n}, \quad \ldots, \quad z_{n-1} = \frac{(n-1)l}{n}, \quad z_n = l \end{aligned} \tag{27}$$

where i is the index identifying the segment and l denotes the total length of the beam.

The boundaries of segment i are defined by:

$$z_{i-1} \le z \le z_i, \quad i = 1, 2, \ldots, n \tag{28}$$

The average value theorem is then applied within each segment to compute effective properties:

$$\bar{f_i} = \frac{1}{z_i - z_{i-1}} \int_{z_{i-1}}^{z_i} f(z)\, dz \tag{29}$$

where $f(z)$ denotes a property function of the beam, $\bar{f_i}$ indicates the average value of segment i and z_{i-1} and z_i are the bounds of the ith segment. By averaging the properties over each segment, it would be possible to represent the complex variability of the beam into a simplified series of constant-property regions without compromising on the accuracy. The segmentation and averaging approach is schematically shown in Fig. 2.

$$\mathbf{Y} = \begin{bmatrix}
1 & 0 & 0 & 0 & z & 0 & \frac{z}{GAk_x} - \frac{I_x z^3}{6E(I_{xy}^2 - I_x I_y)} & \frac{I_{xy} z^3}{6E(I_{xy}^2 - I_x I_y)} & 0 & \frac{-I_{xy} z^2}{2E(I_{xy}^2 - I_x I_y)} & \frac{-I_x z^2}{2E(I_{xy}^2 - I_x I_y)} & 0 \\
0 & 1 & 0 & -z & 0 & 0 & \frac{I_{xy} z^3}{6E(I_{xy}^2 - I_x I_y)} & \frac{z}{GAk_y} - \frac{I_y z^3}{6E(I_{xy}^2 - I_x I_y)} & 0 & \frac{I_y z^2}{2E(I_{xy}^2 - I_x I_y)} & \frac{I_{xy} z^2}{2E(I_{xy}^2 - I_x I_y)} & 0 \\
0 & 0 & 1 & 0 & 0 & 0 & 0 & 0 & \frac{z}{EA} & 0 & 0 & 0 \\
0 & 0 & 0 & 1 & 0 & 0 & \frac{-I_{xy} z^2}{2E(I_{xy}^2 - I_x I_y)} & \frac{I_y z^2}{2E(I_{xy}^2 - I_x I_y)} & 0 & \frac{-I_y z}{E(I_{xy}^2 - I_x I_y)} & \frac{-I_{xy} z}{E(I_{xy}^2 - I_x I_y)} & 0 \\
0 & 0 & 0 & 0 & 1 & 0 & \frac{-I_x z^2}{2E(I_{xy}^2 - I_x I_y)} & \frac{I_{xy} z^2}{2E(I_{xy}^2 - I_x I_y)} & 0 & \frac{-I_{xy} z}{E(I_{xy}^2 - I_x I_y)} & \frac{-I_x z}{E(I_{xy}^2 - I_x I_y)} & 0 \\
0 & 0 & 0 & 0 & 0 & 1 & 0 & 0 & 0 & 0 & 0 & \frac{z}{GI_t} \\
0 & 0 & 0 & 0 & 0 & 0 & 1 & 0 & 0 & 0 & 0 & 0 \\
0 & 0 & 0 & 0 & 0 & 0 & 0 & 1 & 0 & 0 & 0 & 0 \\
0 & 0 & 0 & 0 & 0 & 0 & 0 & -z & 0 & 1 & 0 & 0 \\
0 & 0 & 0 & 0 & 0 & 0 & z & 0 & 0 & 0 & 1 & 0 \\
0 & 0 & 0 & 0 & 0 & 0 & 0 & 0 & 0 & 0 & 0 & 1
\end{bmatrix} \tag{26}$$

Box II.

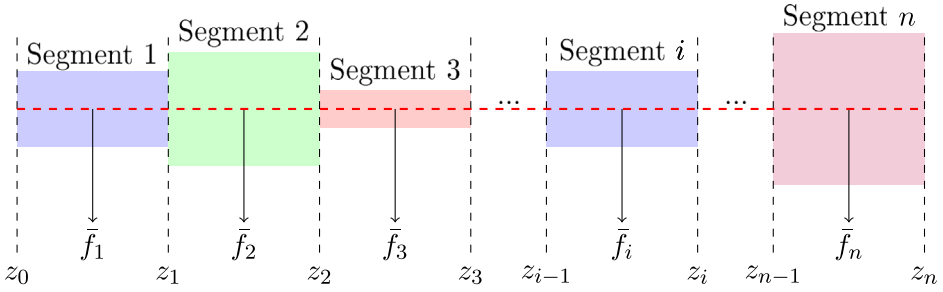

Fig. 2. Schematic visualisation of segmentation and averaging process for beam properties with different geometric and material properties. Different colours indicate different material properties.

In segment i, the system matrix is approximated as constant:

$$\frac{d\mathbf{y}_i(z)}{dz} = \mathbf{A}_i \mathbf{y}_i(z), \quad z_{i-1} \le z \le z_i \tag{30}$$

where $\mathbf{A}_i$ is the constant coefficient matrix associated with the ith segment.

Since the equation is a system of first-order linear ODEs with constant coefficients, its solution in the ith segment can be expressed as:

$$\mathbf{y}_i(z) = e^{\mathbf{A}_i z}\mathbf{y}_{0i}, \quad z_{i-1} \le z \le z_i \tag{31}$$

or in matrix notation:

$$\mathbf{y}_i(z) = \mathbf{Y}_i(0,z)\mathbf{y}_{0i}, \quad \text{where} \quad \mathbf{Y}_i(0,z) = e^{\mathbf{A}_i z} \tag{32}$$

Here, $\mathbf{Y}_i(0,z)$ is the fundamental solution matrix for the segment i.

2.5.3. Boundary and continuity conditions

The transition across segments and enforcement of boundary conditions are governed by the initial values formulation:

$$\mathbf{y}_1(z) = e^{\mathbf{A}_1 z}\mathbf{y}_{01} \tag{33}$$

At the root ($z = 0$):

$$e^{\mathbf{A}_1 0} = \mathbf{I} \tag{34}$$

where $\mathbf{I}$ is the identity matrix. Thus, Eq. (34) becomes:

$$\mathbf{y}_1(0) = \mathbf{y}_{01} \tag{35}$$

Here, 6 components of each boundary vector are known.

For a clamped boundary (fixed end/root), displacements and rotations are zero:

$$u_r = v_r = w_r = \Omega_{xr} = \Omega_{yr} = \Omega_{zr} = 0 \tag{36}$$

and the force and moment resultants F_{xr}, F_{yr}, F_{zr}, M_{xr}, M_{yr}, and M_{zr} are unknown support reactions that must be calculated. Here, the subscript r stands for the root.

For a free end (the tip of the blade):

$$F_{xt}, F_{yt}, F_{zt}, M_{xt}, M_{yt}, M_{zt} \tag{37}$$

are determined by the external loads. Here, the subscript t indicates the tip. While u_t, v_t, w_t, Ω_{xt}, Ω_{yt}, and Ω_{zt} are unknown displacements and rotations which need to be calculated.

The continuity conditions across segments, which ensure that the state vector remains continuous at the interfaces between adjacent segments, also account for the concentrated loads applied at the segment boundaries. This is shown as:

$$\mathbf{y}_{i-1}(z_i) = \mathbf{y}_i(z_i) + \mathbf{K}_i \tag{38}$$

where $\mathbf{K}_i$ is the external concentrated load vector at coordinate z_i that has the dimensions of 12×1 and it can be described as:

$$\mathbf{K}_i^T = \left[0, 0, 0, 0, 0, 0, F_{xi}, F_{yi}, F_{zi}, M_{xi}, M_{yi}, M_{zi}\right] \tag{39}$$

Then, explicitly formulating the continuity conditions yields:

$$e^{\mathbf{A}_{i-1} z_i}\mathbf{y}_{0(i-1)} = e^{\mathbf{A}_i z_i}\mathbf{y}_{0i} + \mathbf{K}_i \tag{40}$$

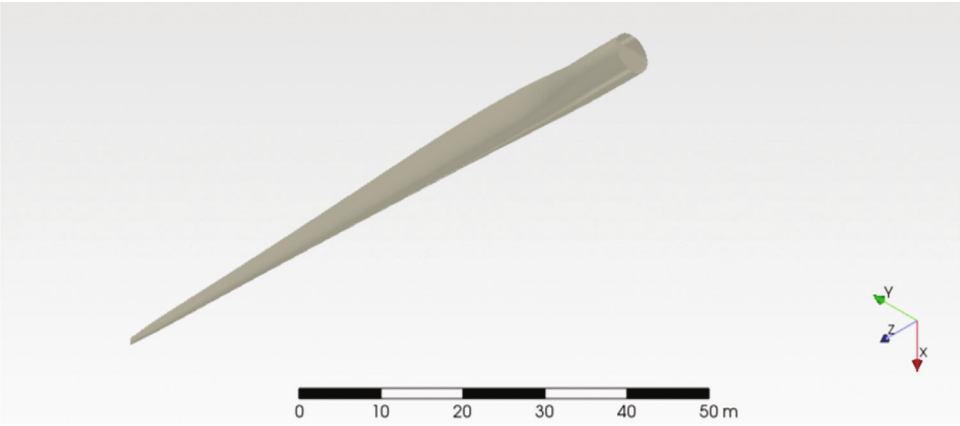

Fig. 3. A view of the computer model of the DTU 10-MW reference wind turbine blade.

2.5.4. Assembly of continuity and boundary conditions

Each block equation has dimension 12×12, and all continuity and boundary conditions can be assembled into the global system:

$$\mathbf{Y}_G\ \mathbf{y}_G = \mathbf{b}_G \tag{41}$$

where:

- $\mathbf{Y}_G \in \mathbb{R}^{12n\times 12n}$ is the global fundamental matrix. Here the subscript G stands for global.
- $\mathbf{y}_G \in \mathbb{R}^{12n\times 1}$ is the unknown vector of all segment initial values $\mathbf{y}_{0i}$
- $\mathbf{b}_G \in \mathbb{R}^{12n\times 1}$ is the right-hand side containing the concentrated loading and the prescribed boundary conditions

The global fundamental matrix $\mathbf{Y}_G$ is given below:

$$\mathbf{Y}_G = \begin{bmatrix} \mathbf{X1} & \mathbf{01} & \cdots & \mathbf{01} \\ -e^{\mathbf{A}_1 z_1} & e^{\mathbf{A}_2 z_1} & \cdots & \mathbf{02} \\ \mathbf{02} & -e^{\mathbf{A}_2 z_2} & \ddots & \vdots \\ \vdots & \ddots & \ddots & \mathbf{02} \\ \mathbf{02} & \cdots & -e^{\mathbf{A}_{n-1} z_{n-1}} & e^{\mathbf{A}_n z_{n-1}} \\ \mathbf{01} & \cdots & \mathbf{01} & \mathbf{X2} \end{bmatrix} \tag{42}$$

In this matrix, **X1** corresponds to the first six rows of $e^{\mathbf{A}_1 0}$, and **X2** corresponds to the last six rows of $e^{\mathbf{A}_n l}$ due to the boundary conditions of the blade being modelled as clamped-free. The symbol **01** denotes a zero matrix of size 6×12, while **02** denotes a zero matrix of size 12×12.

Then the solution vector and right-hand side are:

$$\mathbf{y}_G = \begin{bmatrix} \mathbf{y}_{01} \\ \mathbf{y}_{02} \\ \vdots \\ \mathbf{y}_i \\ \vdots \\ \mathbf{y}_{0n} \end{bmatrix}, \quad \mathbf{b}_G = \begin{bmatrix} \mathbf{K}_r \\ \mathbf{K}_1 \\ \vdots \\ \mathbf{K}_i \\ \vdots \\ \mathbf{K}_t \end{bmatrix} \tag{43}$$

Here, $\mathbf{K}_r$ is a 6×1 vector corresponding to the boundary condition at the root, and is zero since the first six rows are taken. Similarly, $\mathbf{K}_t$ is a 6×1 vector representing the boundary condition at the tip, and it includes tip external loads as the last six rows are taken.

This formulation results in a linear system with $12n$ unknowns and $12n$ equations, incorporating both continuity and boundary constraints. By solving Equation (41), initial values vector $\mathbf{y}_G$ is obtained. This vector $\mathbf{y}_G$ consists of $\mathbf{y}_{0i}$ which is the initial value vector of segment i. Having obtained $\mathbf{y}_{0i}$ for each segment, the analytical solutions can be formulated by using Eq. (31).

The importance/significance of this segmentation approach can be summarised as follows:

- **Simplification of Complex Problems**: By dividing the beam into segments with constant properties, the original complex problem, characterised by variable coefficients in the governing differential equations, is transformed into a set of simpler sub-problems. These sub-problems can often be represented by differential equations with constant coefficients, which are easier to solve and provide a more straightforward pathway to analytical solutions.
- **Improved Accuracy**: Averaging properties within each segment ensures that the overall behaviour of the beam is accurately captured, even with significant variability in geometric and material properties.
- **Flexibility**: This method can be applied to beams with any variation in properties, making it a versatile tool for analysing a wide range of beam configurations.

This segmentation and averaging process is critical for the accurate representation and analysis of beams with variable properties, ensuring that the proposed analytical model can handle complex, real-world engineering systems efficiently and accurately. Therefore, the segment sizes must be arranged accordingly to maintain the model's accuracy and reliability. A convergence analysis might be necessary to ensure the accuracy of the constructed model.

3. Numerical example: DTU 10 MW composite wind turbine blade

To validate this formulation, an example from a paper published by Blasques et al. (2016) is used. That research also proposes an approach that models composite wind turbine blades as beams and compares their approach to a full-scale FE model consisting of shell elements. Specifically, the numerical example focuses on the DTU 10-MW composite wind turbine blade, a well-documented and publicly available model developed by the DTU in collaboration with Vestas Wind Systems (Bak et al., 2013). This blade model is characterised by its non-uniform geometry and the use of composites and FGMs, which are very useful for meeting the operational requirements and achieving the necessary structural efficiency of large-scale wind turbine blades.

The DTU 10-MW wind turbine blade has a complex structural form that incorporates aerofoil designs and is supported by internal beams. The blade's cross-section geometry is optimised for both aerodynamic and structural performance, making it an ideal case study for validating the proposed analytical formulation for non-uniform and asymmetrical beams. The blade and its cross-section are illustrated in Figs. 3 and 4.

To represent the blade using the analytical model, the DTU 10-MW wind turbine blade is segmented into sections, each assumed to have constant properties. These properties are derived by averaging functions that represent the actual variations in geometry and material characteristics along the blade's length. BECAS, an open-source software, is employed in this process by extracting the cross-sectional

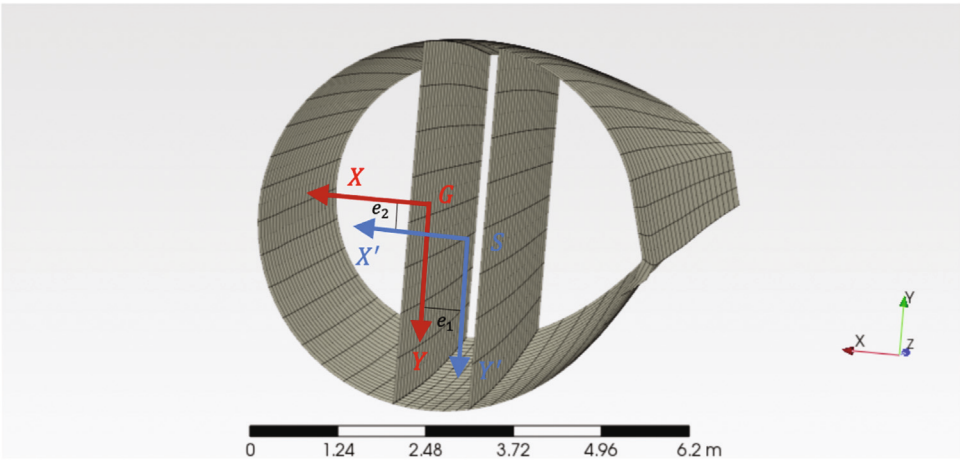

Fig. 4. Description of the asymmetric cross-section.

Table 1
Loading scenarios BLC1 and BLC2 used for validation of the DTU 10-MW blade, as reported by Blasques et al. (2016).

Load Case	Quantity	Spanwise Position z [m]								
		20.1	30.4	33.0	47.7	52.0	62.4	65.8	76.2	84.8
BLC1	F_x [kN]	0.0	0.0	290.0	180.0	0.0	130.0	0.0	18.0	25.0
	F_y [kN]	230.0	270.0	0.0	0.0	250.0	0.0	220.0	190.0	165.0
	M_z [kNm]	−122.7	−226.5	−27.1	−8.0	−170.8	−0.6	−111.9	−74.0	−46.9
BLC2	Position z [m]	89.166								
	M_z [kNm]	450								

properties of the blade. BECAS provides detailed data on the material and geometric properties of the blade's cross-section, which are then used to curve fit the functions that describe these variations along the blade as previously done by Tüfekci et al. (2020). The blade is modelled using 100 segments along its axis, with properties averaged based on 10 points sampled within each segment (Tüfekci et al., 2020).

The comparison between the models of the DTU 10-MW reference blade includes critical assessments of its global response, displacement, and localised strain behaviour under two benchmark loading scenarios, namely BLC1 and BLC2, as defined by Blasques et al. (2016). These loads are applied at specified stations along the blade and are not restricted to tip loading. The specific loads applied in these scenarios – including edgewise force, F_x, flapwise force, F_y, and torsional moment, M_z – are summarised in Table 1. The boundary condition for all models (analytical and FE) assumes a fixed-free configuration, where the root of the blade is clamped and the remainder is left unconstrained.

- **Flapwise Bending and Axial Force (BLC1)**: This loading case is designed to simulate the aerodynamic loading scenario by applying a combination of concentrated transverse forces (F_y) and (F_x), and torsional moments (M_z) at multiple stations along the blade span. These loads are applied at the half-chord location of the cross-sections to emulate realistic aerodynamic effects. Due to the geometric offset between the nodal positions of the beam model and the actual load application point, additional torsional moments are applied exclusively in the beam finite element model to maintain equivalence with the shell model. The distributed nature of the forces makes BLC1 suitable for capturing bending and axial behaviours under operational conditions.
- **Tip Torsional Moment (BLC2)**: In this case, a single torsional moment of 450 kNm is applied at $z = 89.166$ m, which corresponds to the tip of the blade. This scenario evaluates the torsional stiffness and deformation characteristics of the blade, demonstrating the structural response under torsional loads.

The inclusion of both BLC1 and BLC2 load cases enables a comprehensive validation of the proposed analytical beam model across different deformation modes. BLC1 reflects a realistic operational scenario involving complex load distributions that test the model's ability to capture flapwise bending, axial tension/compression, and torsional coupling effects. In contrast, BLC2 isolates the blade's torsional response, serving as a benchmark for evaluating the accuracy of torsional stiffness representation. By applying these cases to both the analytical beam model and the high-fidelity shell-based finite element model under identical boundary conditions, the comparison assesses not only the global displacement fields but also local strain behaviours. This validation approach thus provides a rigorous benchmark for verifying the predictive capabilities of the beam formulation across a broad range of mechanical behaviours.

The proposed analytical model's computational performance and accuracy are evaluated through convergence and CPU time analysis. The solution is implemented as a computer program in Python 3.8.12 and executed on an iMac (Retina 5K, 27-inch, Late 2014) with a Quad-Core Intel Core i7 processor running at 4 GHz, 32 GB of memory, and an AMD Radeon R9 M290X GPU with 2 GB of VRAM. This computational setup ensures the model's performance is evaluated under conditions typical of a desktop environments.

The focus of this assessment is on how the number of segments affects the computational efficiency and accuracy of the model. This evaluation is crucial for demonstrating the practical applicability of the analytical model, considering the computational resource requirements and the precision of the results.

4. Results and discussion for the numerical example

4.1. Overall behaviour of the wind turbine blade: Displacement field

The analytical approach proposed in this study is validated by comparing its results with those obtained from BECAS and shell methods,

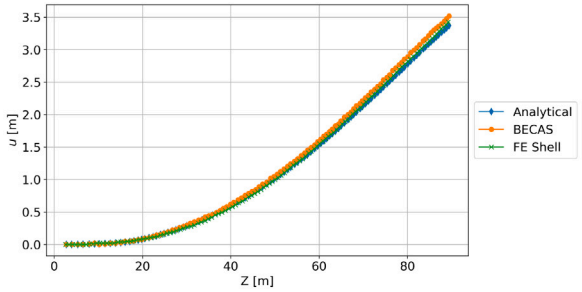

(a) Comparison for u [m] in Load Case BLC1 (Edgewise Displacement).

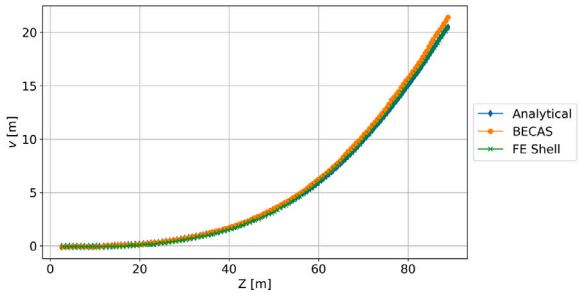

(b) Comparison for v [m] in Load Case BLC1 (Flapwise Displacement).

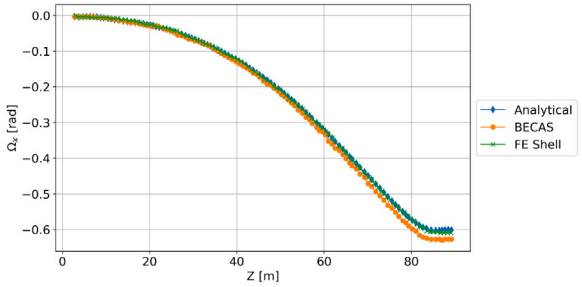

(c) Comparison for flapwise rotation, Ω_x [rad] in Load Case BLC1 (Flapwise Rotation).

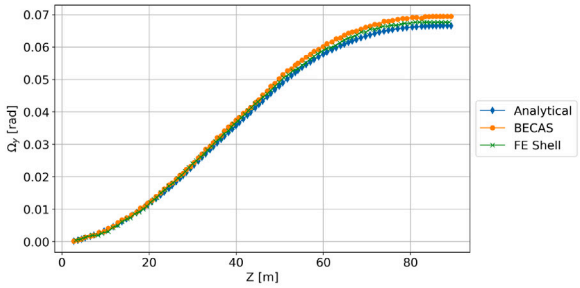

(d) Comparison for edgewise rotation, Ω_y [rad] in Load Case BLC1 (Edgewise Rotation).

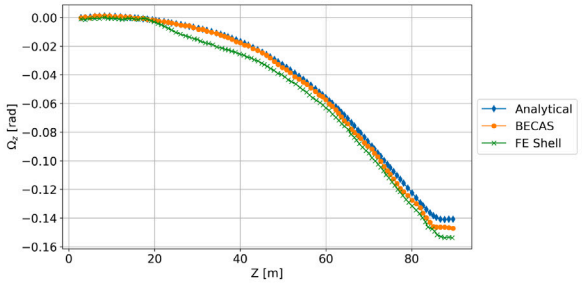

(e) Comparison for torsional rotation, Ω_z [rad] in Load Case BLC1 (Torsional Rotation).

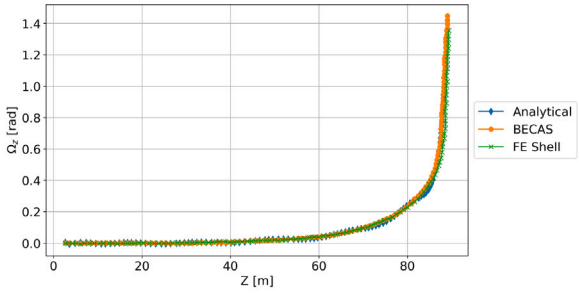

(f) Comparison for torsional rotation, Ω_z [rad] in Load Case BLC2 (Torsional Rotation).

Fig. 5. Comparison of BECAS, full-scale FE with shell elements, and the analytical results (Blasques et al., 2016).

which are well-documented in the literature. Fig. 5 presents comparisons of displacement and rotation results along the length of the wind turbine blade under different load cases. The plots address Load Case BLC1, which involves flapwise bending, edgewise bending, and axial displacement, and Load Case BLC2, which focuses on torsional loading. The displacements in the x- and y-directions, as well as the rotations about the x-, y-, and z-axes, are analysed in terms of u, v, and Ω_x, Ω_y, Ω_z, respectively.

Fig. 5(a) shows the edgewise displacement u along the blade length for Load Case BLC1. The analytical approach demonstrates excellent agreement with both BECAS and shell methods, particularly in the linear region up to approximately 60 metres. Minor deviations observed near the tip are attributed to geometric non-uniformities. The maximum error remains below 5%, indicating strong predictive capability.

In Fig. 5(b), the flapwise displacement v for Load Case BLC1 is shown. The analytical results closely match those of BECAS and the shell model, with only small differences near the blade tip. These discrepancies are within acceptable limits for engineering analysis, with a maximum error around 3%.

Fig. 5(c) presents the flapwise rotation Ω_x for Load Case BLC1. The proposed analytical model captures the rotational response well, following the BECAS and shell results closely. Slight deviations appear near the free end but remain minor. The maximum error is slightly less than 5%.

Fig. 5(d) shows the edgewise rotation Ω_y for Load Case BLC1. The analytical model aligns well with the literature data, especially in the mid-span region. Deviations near the root and tip are minimal, and the maximum error is under 6%.

In Fig. 5(e), the torsional rotation Ω_z for Load Case BLC1 is shown. The analytical prediction follows the general trend of both reference models, although small oscillations appear in the relative difference curve. The overall behaviour is well captured, with the maximum error remaining below 7%.

Finally, Fig. 5(f) shows the torsional rotation Ω_z for Load Case BLC2. The analytical model again matches well with BECAS and the shell solution, with only small differences near the blade tip. While the analytical model appears slightly stiffer, it effectively reproduces the overall structural response. The maximum error is approximately 4%.

One notable observation is that the analytical beam solution appears smoother compared to the other models. This smoothness can be attributed to several factors. First, the geometric and material properties in the analytical model are defined using curve-fitted functions, ensuring a continuous representation of these properties along the beam. In contrast, the other models, particularly those using BECAS, define material properties in a more discontinuous manner, which can introduce abrupt changes and thus less smooth results. Additionally, as a beam model, the analytical approach inherently ensures continuity at the segment boundaries due to the transition conditions between

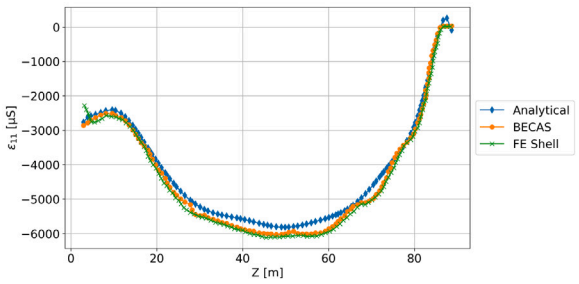

(a) Comparison for ε_{11} in the axial direction for load case BLC1.

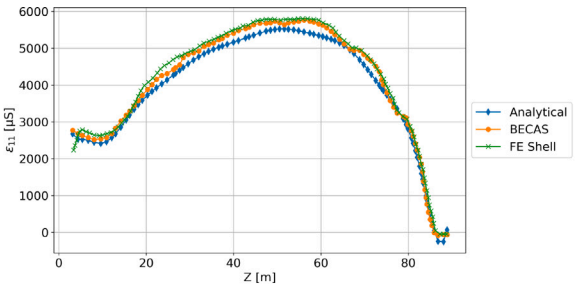

(b) Comparison for ε_{11} in the transverse direction for load case BLC1.

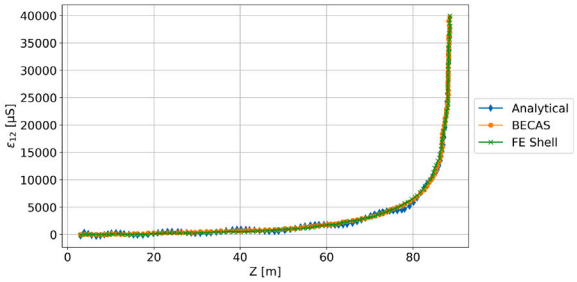

(c) Comparison for ε_{12} (shear strain) for load case BLC2.

Fig. 6. Comparison of localised strain results between the analytical model, BECAS, and the FE shell method.

each segment. This continuity in the solution further contributes to the smoothness of the results, providing a more refined and consistent prediction of the blade's behaviour.

4.2. Localised characteristics of the blade: Strain at cross-sections based of local fibre directions

In addition to the displacement and rotational behaviour, the localised strain distribution across different cross-sections of the wind turbine blade provides more information about the blade's structural characteristics including structural integrity. ε_{11} refers to the axial strain component that is aligned with the local fibre direction and ε_{12} indicates shear strain between fibre and transverse directions. Fig. 6 illustrates the comparison between the strain values obtained using the proposed analytical approach, BECAS, and FE shell models. These comparisons are made to further validate the analytical model's ability to capture local behaviour alongside the global behaviour, particularly in regions of interest where stress and strain concentrations are critical.

Fig. 6(a) presents the strain distribution in the local fibre direction, ε_{11}, under Load Case BLC1. The results show excellent agreement between the analytical model, BECAS, and the shell FE method, with all three approaches following the same trend along the blade length. The analytical model accurately captures the peak strain near the mid-span, with deviations remaining below 5%, demonstrating the reliability of the proposed method in predicting local strain concentrations. Slightly lower magnitudes calculated by the analytical model are expected due to its assumption that the cross-section remains rigid, leading to less deformation and hence lower strain values than the more compliant shell FE model that actually captures the deformation of the blade's cross-sections.

In Fig. 6(b), the transverse axial strain along the local fibre direction, ε_{11}, under Load Case BLC1 is compared across the three methods. The analytical approach again shows a strong correlation with the results from BECAS and the shell FE method, particularly in the regions near the blade root and tip. The differences observed are minimal, and the maximum error is approximately 4%, which is within acceptable engineering limits for this type of analysis. As in the previous case, the slightly lower strain values from the analytical model are expected due to the rigid cross-section assumption.

Finally, the shear strain, ε_{12}, under Load Case BLC2 is shown in Fig. 6(c). The shear strain results highlight the analytical model's ability to capture the blade's response to torsional loading. The agreement between the analytical model, BECAS, and the FE shell method is excellent, with deviations of less than 5% along the blade length, particularly near the blade tip where shear effects are significant. The reduced strain magnitudes calculated by the analytical model are, once again, attributed to the assumption that cross-sections remain rigid and undeformed, leading to lower strain estimates compared to the shell FE results, which account for cross-sectional deformations.

The comparison of calculated strain values reinforces the validity of the proposed analytical model in predicting both the global and localised behaviour of the wind turbine blade. The excellent agreement with BECAS and FE methods, particularly in critical regions, highlights the model's robustness and practical applicability for large-scale wind turbine blade analyses. The slightly lower strain values predicted by the analytical model are consistent with the assumption of a rigid cross-section, which leads to less deformation and hence lesser strain values compared to more compliant FE model.

4.3. Convergence and CPU time analysis

In this section, the convergence behaviour and computational performance of the proposed analytical model are discussed considering the impact of the number of segments on the accuracy of the results of the first loading scenario BLC1. Additionally, the CPU time required for computations is evaluated.

Fig. 7(a) illustrates the error in the calculated tip displacement magnitudes as a function of the number of segments. The error is computed using the tip displacement magnitudes obtained with 500 segments as the reference value. It can be observed that the error decreases significantly as the number of segments increases, demonstrating the convergence of the model. Notably, the maximum error is reduced to below 5% when the number of segments exceeds 100, indicating that the model provides accurate results with sufficient segmentation. The observed stiffness in the analytical model, attributed to the neglect of cross-sectional deformation, is evident in the error reduction trend. Despite this, the analytical model captures the overall system behaviour accurately.

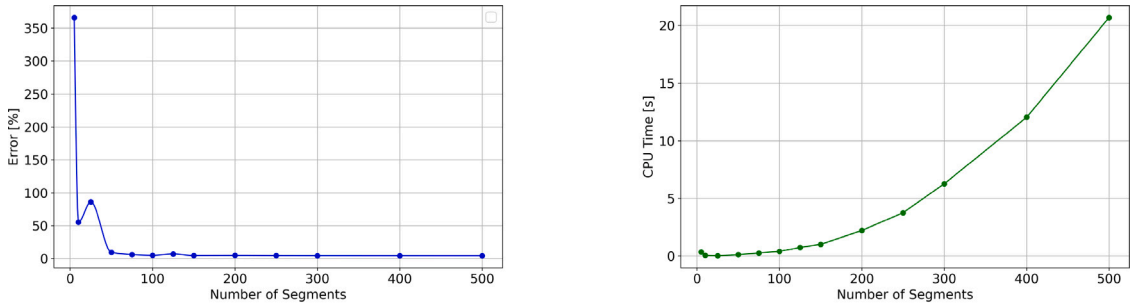

(a) Error vs Number of Segments (b) CPU Time vs Number of Segments

Fig. 7. Convergence and CPU time analysis for the proposed analytical model for BLC1.

Fig. 7(b) presents the CPU time required for computations with varying numbers of segments. It is clear that the computational time increases with the number of segments. The relationship between the number of segments and CPU time is approximately quadratic, which is consistent with the expected computational complexity for this type of analysis. For practical applications, a balance between accuracy and computational efficiency must be considered, with the number of segments chosen to ensure acceptable accuracy while maintaining manageable computation times.

5. Conclusion

This study presents a novel analytical approach for analysing non-uniform and asymmetrical beams made of functionally graded materials (FGMs), with validation provided through a detailed numerical example involving the DTU 10-MW composite wind turbine blade. The key contributions of this work include the formulation of equilibrium, compatibility, and constitutive equations that effectively capture the complex interactions within beams with varying properties along their length.

The DTU 10-MW composite wind turbine blade served as an ideal test case due to its intricate geometry and material heterogeneity. To ensure accurate representation, the blade was segmented into regions with constant properties, and the geometric and material characteristics within each segment were averaged. These properties were extracted using BECAS, an open-source tool designed for analysing anisotropic and inhomogeneous beam cross-sections, which played a critical role in curve-fitting the variation of these properties along the blade's axis.

The performance of the proposed analytical model was validated against results from BECAS and full-scale shell FE models from the literature. Excellent agreement was observed in strain, displacement and rotational responses along the blade length, with a maximum error of consistently below 7%. This validation demonstrates the accuracy and robustness of the proposed analytical model in capturing the overall system behaviour, despite the model's inherent simplifications.

Additionally, the computational performance of the analytical model was evaluated through a detailed convergence and CPU time analysis. The error in the calculated tip displacement magnitudes decreased significantly as the number of segments increased, with sufficient accuracy achieved using more than 100 segments. The CPU time analysis indicated a quadratic relationship between the number of segments and computation time, demonstrating that the analytical model offers a balance between accuracy and computational efficiency, making it suitable for practical engineering applications.

Even though the proposed analytical model has been successfully validated against the DTU 10-MW wind turbine blade case, which features non-uniform geometry and material heterogeneity, certain limitations remain when applying the model to more complex structural configurations. Specifically, blades that exhibit significant twist, taper, or include multi-cell transverse cross-sections, as well as those with spatially varying locations of centroids, shear centres, torsional axes, and flexural axes, may introduce deformation modes and coupling effects that extend beyond the capabilities of the current formulation. These complex features can lead to intricate three-dimensional stress states and local behaviours that are not fully captured by the present beam-based approach. Future work may address these challenges by incorporating more advanced cross-sectional modelling techniques or extending the theory to account for such geometrical complexities.

Overall, the results demonstrate that the proposed analytical approach is both effective and reliable for the analysis of non-uniform and asymmetrical beams made of functionally graded materials. The agreement with well-established numerical methods further validates the model's applicability, particularly for the design and optimisation of large-scale wind turbine blades. The consistent maximum error of below 7% across all comparisons highlights the model's accuracy and practical relevance.

Finally, the proposed analytical model exhibits strong convergence characteristics and reasonable computational demands. The results indicate that the model can reliably predict the structural behaviour of non-uniform and asymmetrical beams, which offers significant advantages for engineering applications, particularly in the design and optimisation of wind turbine blades. Future work could extend this approach to include local stress and strain assessments, improving the model's applicability and precision for even more complex structural analyses.

CRediT authorship contribution statement

Mertol Tüfekci: Writing – review & editing, Writing – original draft, Visualization, Validation, Software, Resources, Methodology, Investigation, Formal analysis, Conceptualization. **Ekrem Tüfekci:** Writing – review & editing, Validation, Resources, Methodology, Investigation, Conceptualization.

Declaration of competing interest

The authors declare that they have no known competing financial interests or personal relationships that could have appeared to influence the work reported in this paper.

Data availability

No data was used for the research described in the article.

References

Artan, R., Tepe, A., 2025a. In-plane static behavior of nonlocal curved nanobeams resting on an elastic foundation determined using the initial value method. J. Elasticity 157 (3), http://dx.doi.org/10.1007/s10659-025-10140-w.

Artan, R., Tepe, A., 2025b. Out-of-plane static analysis of curved nanobeams resting on an elastic foundation using the method of initial values. ZAMM Zeitschrift_s*für Angew. Math. Und Mech. 105 (5), 1–16. http://dx.doi.org/10.1002/zamm.70031.

Avcar, M., Hadji, L., Civalek, Ö., 2021. Natural frequency analysis of sigmoid functionally graded sandwich beams in the framework of high order shear deformation theory. Compos. Struct. 276, 114564. http://dx.doi.org/10.1016/j.compstruct.2021.114564, URL https://linkinghub.elsevier.com/retrieve/pii/S0263822321010266.

Bak, C., Zahle, F., Bitsche, R., Kim, T., Yde, A., Henriksen, L.C., Hansen, M.H., Blasques, J.P.A.A., Gaunaa, M., Natarajan, A., 2013. The DTU 10-MW reference wind turbine.

Barnes, R.H., Morozov, E.V., 2016. Structural optimisation of composite wind turbine blade structures with variations of internal geometry configuration. Compos. Struct. 152, 158–167. http://dx.doi.org/10.1016/j.compstruct.2016.05.013, URL http://dx.doi.org/10.1016/j.compstruct.2016.05.013.

Bechly, M., Clausen, P., 1997. Structural design of a composite wind turbine blade using finite element analysis. Comput. Struct. 63, 639–646. http://dx.doi.org/10.1016/s0045-7949(96)00387-2.

Blasques, P., 2012. User manual for BECAS (executable version) a cross section analysis tool for anisotropic and inhomogeneous beam sections of arbitrary geometry. In: DTU Orbit. pp. 1–26.

Blasques, J.P., Bitsche, R.D., Fedorov, V., Lazarov, B.S., 2016. Accuracy of an efficient framework for structural analysis of wind turbine blades. Wind. Energy 19 (9), 1603–1621. http://dx.doi.org/10.1002/we.1939, URL https://onlinelibrary.wiley.com/doi/10.1002/we.1939.

Branner, K., Blasques, J.P., Kim, T., Fedorov, V.A., Berring, P., Bitsche, R.D., Berggreen, C., Branner, K., Blasques, J.P., Kim, T., Fedorov, V.A., 2012. Anisotropic beam model for analysis and design of passive controlled wind turbine blades. In: DTU WInd Energy. vol. 0001, (February), pp. 1–41. http://dx.doi.org/10.13140/RG.2.2.33863.29606, URL https://www.researchgate.net/publication/307957381%0AAnisotropic.

Brøndsted, P., Lilholt, H., Lystrup, A., 2005. Composite materials for wind power turbine blades. Annu. Rev. Mater. Res. 35, 505–538. http://dx.doi.org/10.1146/annurev.matsci.35.100303.110641.

Buckney, N., Pirrera, A., Green, S.D., Weaver, P.M., 2013. Structural efficiency of a wind turbine blade. Thin-Walled Struct. 67, 144–154. http://dx.doi.org/10.1016/j.tws.2013.02.010.

Cao, D., Bouzolin, D., Lu, H., Griffith, D.T., 2023. Bending and shear improvements in 3D-printed core sandwich composites through modification of resin uptake in the skin/core interphase region. Compos. Part B: Eng. 264, 110912. http://dx.doi.org/10.1016/j.compositesb.2023.110912, URL https://linkinghub.elsevier.com/retrieve/pii/S1359836823004158.

Cardenas, D., Escárpita, A., Elizalde, H., Aguirre, J., Ahuett, H., Marzocca, P., Probst, O., Ahuett-Garza, H., 2011. Numerical validation of a finite element thin-walled beam model of a composite wind turbine blade. Wind. Energy 15, 203–223. http://dx.doi.org/10.1002/we.462.

Chang, L., Yu, Y., Liu, T., 2020. Aeroelastic flutter and sliding mode control of wind turbine blade. Shock. Vib. 2020, 1–8. http://dx.doi.org/10.1155/2020/8846529.

Chen, X., Tang, J., Yang, K., 2019. Modeling multiple failures of composite box beams used in wind turbine blades. Compos. Struct. http://dx.doi.org/10.1016/J.COMPSTRUCT.2019.03.018.

Chortis, D.I., Chrysochoidis, N.A., Saravanos, D.A., 2007. Damped structural dynamics models of large wind-turbine blades including material and structural damping. J. Phys.: Conf. Ser. 75 (1), http://dx.doi.org/10.1088/1742-6596/75/1/012076.

Couturier, P.J., Krenk, S., 2016. Wind turbine cross-sectional stiffness analysis using internally layered solid elements. AIAA J. 54 (7), 2149–2159. http://dx.doi.org/10.2514/1.J054543.

Eder, M.A., Bitsche, R.D., 2015. A qualitative analytical investigation of geometrically nonlinear effects in wind turbine blade cross sections. Thin-Walled Struct. 93, 1–9. http://dx.doi.org/10.1016/j.tws.2015.03.007.

Faccio Júnior, C.J., Cardozo, A.C.P., Monteiro Júnior, V., Gay Neto, A., 2019. Modeling wind turbine blades by geometrically-exact beam and shell elements: A comparative approach. Eng. Struct. 180 (March 2018), 357–378. http://dx.doi.org/10.1016/j.engstruct.2018.09.032.

Fagan, E.M., Flanagan, M., Leen, S.B., Flanagan, T., Doyle, A., Goggins, J., 2017. Physical experimental static testing and structural design optimisation for a composite wind turbine blade. Compos. Struct. 164, 90–103. http://dx.doi.org/10.1016/j.compstruct.2016.12.037, URL http://dx.doi.org/10.1016/j.compstruct.2016.12.037.

Filippi, M., Carrera, E., Zenkour, A.M., 2015. Static analyses of FGM beams by various theories and finite elements. Compos. Part B: Eng. 72, 1–9. http://dx.doi.org/10.1016/j.compositesb.2014.12.004, URL http://dx.doi.org/10.1016/j.compositesb.2014.12.004.

Genel, Ö.E., Tüfekci, E., 2023a. Axial–torsional coupled static behavior of inhomogeneous pretwisted cantilever beams. Acta Mech. 234 (8), 3421–3436. http://dx.doi.org/10.1007/s00707-023-03561-y.

Genel, Ö.E., Tüfekci, E., 2023b. Bending-bending coupled static analysis of functionally graded and porous pretwisted cantilever beams using initial values method. Mech. Based Des. Struct. Mach. 1–24. http://dx.doi.org/10.1080/15397734.2023.2185632.

Guan, S., Zhao, J., Dai, L., Zhang, S., Zhao, H., 2023. Static and dynamic mechanical behaviors of bamboo scrimber under combined tension-bending. Compos. Sci. Technol. 242, 110191. http://dx.doi.org/10.1016/j.compscitech.2023.110191, URL https://linkinghub.elsevier.com/retrieve/pii/S0266353823002853.

Guo, S., Li, Y., Chen, W., 2020. Analysis on dynamic interaction between flexible bodies of large-sized wind turbine and its response to random wind loads. Renew. Energy 163, 123–137. http://dx.doi.org/10.1016/j.renene.2020.08.126.

Hadji, L., Avcar, M., Civalek, Ö., 2021. An analytical solution for the free vibration of FG nanoplates. J. Braz. Soc. Mech. Sci. Eng. 43 (9), 418. http://dx.doi.org/10.1007/s40430-021-03134-x, URL https://link.springer.com/10.1007/s40430-021-03134-x.

Jiang, Y., Finnegan, W., Flanagan, T., Goggins, J., 2022a. Optimisation of highly efficient composite blades for retrofitting existing wind turbines. Energies http://dx.doi.org/10.3390/en16010102.

Jiang, B., Hui, Y., Yang, Q., Hua, X., 2022b. Nonlinear dynamic analysis of parked large wind turbine blade considering harmonic inertial excitation using continuum mathematical model. Thin-Walled Struct. 181 (September), 110128. http://dx.doi.org/10.1016/j.tws.2022.110128.

Júnior, C., Cardozo, A., Júnior, V., Neto, A., 2019. Modeling wind turbine blades by geometrically-exact beam and shell elements: A comparative approach. Eng. Struct. 180, 357–378. http://dx.doi.org/10.1016/j.engstruct.2018.09.032.

Jureczko, M., Mrówka, M., 2022. Multiobjective optimization of composite wind turbine blade. Materials 15 (13), 4649. http://dx.doi.org/10.3390/ma15134649, URL https://www.mdpi.com/1996-1944/15/13/4649.

Katili, I., Syahril, T., Katili, A.M., 2020. Static and free vibration analysis of FGM beam based on unified and integrated of Timoshenko's theory. Compos. Struct. 242 (November 2019), 112130. http://dx.doi.org/10.1016/j.compstruct.2020.112130.

Kong, C., Bang, J., Sugiyama, Y., 2005. Structural investigation of composite wind turbine blade considering various load cases and fatigue life. Energy 30, 2101–2114. http://dx.doi.org/10.1016/j.energy.2004.08.016.

Li, L., Li, Y., Liu, Q., Lv, H., 2014. A mathematical model for horizontal axis wind turbine blades. Appl. Math. Model. 38 (11–12), 2695–2715. http://dx.doi.org/10.1016/j.apm.2013.10.068, URL https://linkinghub.elsevier.com/retrieve/pii/S0307904X13007361.

Liu, P., 2021. Explicit finite element analysis of impact-induced damage of composite wind turbine blade under typhoon by considering fluid/solid interaction. In: Damage Modeling of Composite Structures. Elsevier, pp. 297–303. http://dx.doi.org/10.1016/B978-0-12-820963-9.00003-1, URL https://linkinghub.elsevier.com/retrieve/pii/B9780128209639000031.

Liu, J., Liu, P., Leng, J., Wang, C., 2022a. Finite element analysis of damage mechanisms of composite wind turbine blade by considering fluid/solid interaction. Part I: Full-scale structure. Compos. Struct. 301, 116212. http://dx.doi.org/10.1016/j.compstruct.2022.116212, URL https://linkinghub.elsevier.com/retrieve/pii/S0263822322009448.

Liu, P.F., Liu, J.W., Wang, C.Z., Liu, P.F., Leng, J.X., Wang, C.Z., Liu, J.W., Wang, C.Z., 2022b. Finite element analysis of damage mechanisms of composite wind turbine blade by considering fluid/solid interaction. Part II: T-shape adhesive structure. Compos. Struct. 301 (August), 116211. http://dx.doi.org/10.1016/j.compstruct.2022.116211.

Mohamad Mirfatah, S., Salehipour, H., Civalek, Ö., 2024. Geometrically nonlinear vibration of toroidal sandwich shells with auxetic honeycomb core under periodic/impulsive pressure. Compos. Struct. 339, 118166. http://dx.doi.org/10.1016/j.compstruct.2024.118166, URL https://linkinghub.elsevier.com/retrieve/pii/S0263822324002940.

Natarajan, B., Lee, J., Lim, J.-I., Shin, S.-J., 2012. Structural analysis of composite wind turbine blade using advanced beam model approach. Int. J. Precis. Eng. Manuf. 13, 2245–2250. http://dx.doi.org/10.1007/S12541-012-0298-6.

Ozyildiz, M., Muyan, C., Coker, D., 2018. Strength analysis of a composite turbine blade using puck failure criteria. J. Phys.: Conf. Ser. 1037, 042027. http://dx.doi.org/10.1088/1742-6596/1037/4/042027.

Peng, M., Hui, Y., Li, S., Yang, Q., 2024. Nonlinear dynamic analysis of parked large wind turbine blade considering parametric excitation. Thin-Walled Struct. 201 (PB), 112032. http://dx.doi.org/10.1016/j.tws.2024.112032.

Raman, V., Drissi-Habti, M., Guillaumat, L., Khadhour, A., 2016. Numerical simulation analysis as a tool to identify areas of weakness in a turbine wind-blade and solutions for their reinforcement. Compos. Part B: Eng. 103, 23–39. http://dx.doi.org/10.1016/j.compositesb.2016.07.018, URL http://dx.doi.org/10.1016/j.compositesb.2016.07.018.

Schubel, P., Crossley, R., 2012. Wind turbine blade design. Energies 5, 3425–3449. http://dx.doi.org/10.3390/en5093425.

Spini, F., Bettini, P., 2024. End-of-life wind turbine blades: Review on recycling strategies. Compos. Part B: Eng. 275, 111290. http://dx.doi.org/10.1016/j.compositesb.2024.111290, URL https://linkinghub.elsevier.com/retrieve/pii/S135983682400101X.

Tarfaoui, M., Nachtane, M., Boudounit, H., 2020. Finite element analysis of composite offshore wind turbine blades under operating conditions. J. Therm. Sci. Eng. Appl. 12 (1), 1–11. http://dx.doi.org/10.1115/1.4042123, URL https://asmedigitalcollection.asme.org/thermalscienceapplication/article/doi/10.1115/1.4042123/632829/Finite-Element-Analysis-of-Composite-Offshore-Wind.

Tepe, A., 2025. Nonlocal effects on curved double-walled carbon nanotubes based on nonlocal theory. Arch. Appl. Mech. 95 (2), 57. http://dx.doi.org/10.1007/s00419-025-02762-2, URL https://link.springer.com/10.1007/s00419-025-02762-2.

Theotokoglou, E., Balokas, G., 2014. Computational analysis and material selection in cross-section of a composite wind turbine blade. J. Reinf. Plast. Compos. 34, 101–115. http://dx.doi.org/10.1177/0731684414565224.

Thomsen, O., 2009. Sandwich materials for wind turbine blades—Present and future. J. Sandw. Struct. Mater. 11, 7–26. http://dx.doi.org/10.1177/1099636208099710.

Tüfekci, M., 2023. Performance evaluation analysis of ti-6al-4V foam fan blades in aircraft engines: A numerical study. Compos. Part C: Open Access 12, 100414. http://dx.doi.org/10.1016/j.jcomc.2023.100414.

Tüfekci, M., 2025. Forced vibration analysis of rotating blades subjected to large deformations: A numerical investigation with VIBRANT. In: ASME 2025 Aerospace Structures, Structural Dynamics, and Materials Conference. American Society of Mechanical Engineers, pp. 1–10. http://dx.doi.org/10.1115/SSDM2025-152240, URL https://asmedigitalcollection.asme.org/ssdm/proceedings/SSDM2025/88759/V001T02A011/1219029.

Tüfekci, M., Dear, J.P., Salles, L., 2024a. Forced vibration analysis of beams with frictional clamps. Appl. Math. Model. 128 (October 2023), 450–469. http://dx.doi.org/10.1016/j.apm.2024.01.031.

Tufekci, E., Dogruer, O.Y., 2002. Exact solution of out-of-plane free vibrations of a circular beam with uniform cross-section. Int. J. Struct. STability Dyn. 231–236. http://dx.doi.org/10.1142/9789812776228_0028.

Tufekci, E., Dogruer, O.Y., 2006. Exact solution of out-of-plane problems of an arch with varying curvature and cross section. J. Eng. Mech. 132 (6), 600–609. http://dx.doi.org/10.1061/(asce)0733-9399(2006)132:6(600).

Tüfekci, M., Genel, Ö.E., Tatar, A., Tüfekci, E., 2020. Dynamic analysis of composite wind turbine blades as beams: An analytical and numerical study. Vibration 4 (1), 1–15. http://dx.doi.org/10.3390/vibration4010001, URL https://www.mdpi.com/2571-631X/4/1/1.

Tüfekci, M., Kocak, O., Özkan, Y., Pır, İ., Tüfekci, E., 2025. Numerical evaluation of design strategies for a composite wind turbine blade: Using metallic foams and optimising topology. Energy Sci. Eng. 13 (4), 1457–1477, URL https://scijournals.onlinelibrary.wiley.com/doi/10.1002/ese3.70030.

Tufekci, E., Ozdemirci, O., 2006. Exact solution of free in-plane vibration of a stepped circular arch. J. Sound Vib. 295 (3–5), 725–738. http://dx.doi.org/10.1016/j.jsv.2006.01.048.

Tüfekci, M., Öztekin, V., Pir, İ., Alioğlu, M., Dikicioğlu, C., Dikicioğlu, A., Tüfekci, E., 2023. Low strain rate mechanical performance of balsa wood and carbon fibre-epoxy-balsa sandwich structures. Compos. Part C: Open Access 12 (November), 100416. http://dx.doi.org/10.1016/j.jcomc.2023.100416, URL https://linkinghub.elsevier.com/retrieve/pii/S2666682023000725.

Tüfekci, M., Sun, Y., Yuan, J., Maharaj, C., Liu, H., Dear, J.P., Salles, L., 2024b. Analytical vibration modelling and solution of bars with frictional clamps. J. Sound Vib. 577 (January), 118307. http://dx.doi.org/10.1016/j.jsv.2024.118307, https://linkinghub.elsevier.com/retrieve/pii/S0022460X24000713.

Uzun, B., Yaylı, M.Ö., Civalek, Ö., 2024. Vibration of embedded restrained composite tube shafts with nonlocal and strain gradient effects. Acta Mech. 235 (8), 5137–5159. http://dx.doi.org/10.1007/s00707-024-03970-7, URL https://link.springer.com/10.1007/s00707-024-03970-7.

Van Buren, K., Atamturktur, S., 2012. A comparative study: Predictive modeling of wind turbine blades. Wind Eng. 36 (3), 235–250. http://dx.doi.org/10.1260/0309-524X.36.3.235.

Wang, L., Kolios, A., Nishino, T., Delafin, P.L., Bird, T., 2016. Structural optimisation of vertical-axis wind turbine composite blades based on finite element analysis and genetic algorithm. Compos. Struct. 153 (January 2015), 123–138. http://dx.doi.org/10.1016/j.compstruct.2016.06.003, URL http://dx.doi.org/10.1016/j.compstruct.2016.06.003.

Wang, Q., Yu, W., 2017. Geometrically nonlinear analysis of composite beams using Wiener-Milenković parameters. J. Renew. Sustain. Energy 9, 033306. http://dx.doi.org/10.1063/1.4985091.

Xiao, J., Chen, Y., Zhu, Q., Lee, J., Ma, T., 2017. A general ply design for aero engine composite fan blade. Proc. the ASME Turbo Expo 7A-2017, 1–8. http://dx.doi.org/10.1115/GT201764377.

Yilmaz, S., Eken, S., Kaya, M.O., 2014. Dynamic and aeroelastic analyses of a wind turbine blade modeled as a thin-walled composite beam. In: Volume 6B: Energy. American Society of Mechanical Engineers, http://dx.doi.org/10.1115/IMECE2014-38679, https://asmedigitalcollection.asme.org/IMECE/proceedings-abstract/IMECE2014/46521/V06BT07A073/263015 https://asmedigitalcollection.asme.org/IMECE/proceedings/IMECE2014/46521/Montreal, Quebec, Canada/263015.

Yu, W., 2011. VABS manual for users. In: Department of Mechanical and Aerospace Engineering, Utah State University, Logan, Utah. Tech. Rep, pp. 1–22.

Yu, W., Hodges, D.H., Ho, J.C., 2012. Variational asymptotic beam sectional analysis – An updated version. Internat. J. Engrg. Sci. 59, 40–64. http://dx.doi.org/10.1016/j.ijengsci.2012.03.006, URL https://linkinghub.elsevier.com/retrieve/pii/S0020722512000493.

Zheng, T., Chen, N.Z., Yuan, L., 2023. Structural strength assessment for thin-walled blade root joint of floating offshore wind turbine (FOWT). Thin-Walled Struct. 191 (July), 111057. http://dx.doi.org/10.1016/j.tws.2023.111057.

Zhou, X., Huang, K., Li, Z., 2018. Geometrically nonlinear beam analysis of composite wind turbine blades based on quadrature element method. Int. J. Non-Linear Mech. http://dx.doi.org/10.1016/J.IJNONLINMEC.2018.05.007.